Experimental demonstration of radius-varying active plasma lensing for laser-plasma-accelerated proton beams with increased collection angle

Yang Yan,[1,2] Tong Yang,[1,2] Zhen Guo,[1,2] Mingfeng Huang,[1,2] Hao Cheng,[1,2] Yuze Li,[1,2] Yanlv Fang,[1,2] Chentong Li,[1,2] Yadong Xia,[1,2] Qiangyou He,[1,2] Yiting Yan,[1,2] Chen Lin,[1,2,3,*] and Xueqing Yan[1,2,3]

[1]*State Key Laboratory of Nuclear Physics and Technology, and Key Laboratory of HEDP of the Ministry of Education, CAPT, Peking University, Beijing, 100871, China*
[2]*Beijing Laser Acceleration Innovation Center, Huairou, Beijing, 101407, China*
[3]*Institute of Guangdong Laser Plasma Technology, Baiyun, Guangzhou, 510475, China*

(Received 29 November 2023; accepted 16 April 2024; published 13 May 2024)

Active plasma lensing, a compact method for intensifying the focus of charged particle beams by providing a magnetic field gradient of kT/m, has emerged as a sought-after technology in laser plasma accelerator applications. However, the utilization of active plasma lenses faces significant hurdles when dealing with laser-driven proton pulses, characterized by their broad bandwidth and high divergence. To address this challenge, we developed a novel active plasma lens with a variable radius, specifically designed to optimize lens geometry in accordance with the beam envelope, and performed the first measurement of its focusing ability. The experimental findings reveal that, compared to conventional cylindrical active plasma lenses, our radius-varying lens exhibits a 2.0-fold improvement in single-energy transmission efficiency, while maintaining comparable achromatic ability. This breakthrough is anticipated to significantly contribute to the miniaturization of laser proton accelerators.

DOI: 10.1103/PhysRevAccelBeams.27.052802

I. INTRODUCTION

Laser plasma proton acceleration, with its acceleration gradients surpassing traditional accelerators by 3 orders of magnitude [1], has opened vast possibilities for constructing next-generation compact accelerators [2–4] and their applications, such as miniaturized proton therapy devices [5–8] and radiation sources [9]. However, the high gradient and transient nature of this acceleration process also make it susceptible to nonlinearity and instability, resulting in laser-accelerated proton beams characterized by large divergence angles (hundreds of mrad) [10,11] and broad energy spectra (up to 100%). These features present substantial challenges for subsequent beam transport, including the excessively large size of traditional magnetic beamlines [12–14] (compared to the acceleration unit) and the low transmission efficiency of beams [15]. Consequently, research into bespoke transmission components tailored to the laser acceleration mechanism and the unique characteristics of proton beams is imperative. This endeavor requires not only keeping pace with the high electromagnetic field gradients to minimize size but also expanding the collection angle and transmission energy spectrum to facilitate applications with high dose requirements.

Active plasma lensing represents a promising technology that employs a longitudinal current I through plasma-filled capillaries to generate a high-gradient, tunable, and axisymmetric angular magnetic field $B = \mu_0 J r/2$, enabling low-dispersion [16] focusing of laser plasma accelerated (LPA) particle beams within centimeter scales, where μ_0 is the vacuum permeability, and $J = I/\pi R^2$ (assuming that the current is uniformly distributed in the plasma column with a radius of R) is the current density. This concept, first introduced in the 1950s [17], was initially used for transporting large-scale beams with centimeter radii from traditional accelerators. However, its practical use was constrained by excessive power consumption, with operating currents ranging from tens to hundreds of kiloamperes and instability arising from plasma z-pinch movements [18–21]. In 2015, Van Tilborg *et al.* [22] revolutionized this field by proposing active plasma lenses (APLs) based on discharged gas-filled capillaries specifically for LPA electrons. They focused 100-MeV-level LPA electrons using a capillary with a peak current of 330 A and a radius of 125 μm. The small emittance [23] of LPA particles allowed for a significant reduction in APL radius to the order of hundreds of micrometers, drastically lowering the peak current requirements. This allows for the magnetic pressure

*lc0812@pku.edu.cn

within the capillary to be lower than the kinetic pressure [24,25], i.e.,

$$\mu_0 I^2/(8\pi^2 R^2) < n_0 k_B T_e, \quad (1)$$

where n_0 is the plasma density, k_B is the Boltzmann constant, and T_e is the electron temperature. Therefore, the z-pinch effect can be neglected, eliminating the temporal evolution of the plasma column radius and enhancing magnetic field stability.

Later on, several studies have demonstrated the focusing effects of APLs on LPA electron beams [26–32], facilitating research in cutting-edge areas like cascaded acceleration [33]. However, exploration of APL application for focusing LPA proton beams remains limited. The primary challenge lies in the low transmission efficiency: the divergence angles of LPA proton beams are 2 orders of magnitude larger than that of electron beams, resulting in a significant proportion of protons either missing the APLs' entrances or hitting the channel walls and being lost. For instance, the only reported experiment using an APL to guide LPA proton beams showed a collection angle of 11 mrad, and 0.2% of protons (with an initial FWHM divergence of 260 mrad) was transmitted [6]. One method to increase transmission efficiency is by expanding the capillary radius R and proportionally increasing the discharge current $I \propto R^2$ to ensure current density. However, this would increase the cost of circuit construction and operation. Additionally, Eq. (1) indicates an upper limit on the current value to avoid z-pinch effects. Hence, it is imperative to explore other methods to increase the APL collection angle.

We have theoretically demonstrated that this issue could be relieved by dynamically altering the geometry of the APL [34]. In the previous cylindrical APL (C-APL), the constant radius fails to adapt to the changing transverse dimensions of the beam, leading to suboptimal utilization of the discharge current's focusing power. In contrast, our proposed radius-varying APL (RV-APL) optimizes the aperture of the capillary to perfectly align with the beam envelope, thereby enhancing magnetic field utilization and significantly increasing beam transmission efficiency. The geometrical sketch of the C-APL and RV-APL can be found in Fig. 1(a).

In this experiment, we conducted the first comparative tests of C-APL and RV-APL in focusing LPA protons at MeV-level energies. Without altering the external current magnitude and the intended focusing position, RV-APL was observed to expand the acceptance angle range to 1.5 times that of C-APL. This resulted in a doubling of beam density and total charge for protons passing through RV-APL compared to C-APL. Such a compact, dose-enhancing beam transmission component is of significant importance for the development of various applications of laser accelerators.

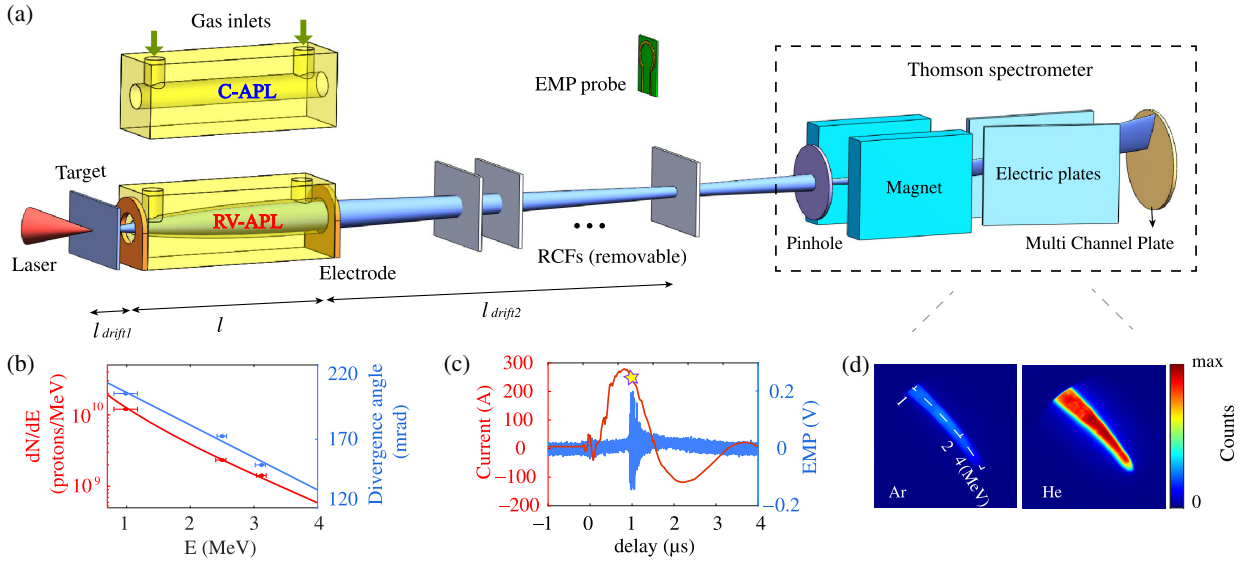

FIG. 1. Experimental setup: (a) Illustration of active plasma lenses (C-APL or RV-APL) focusing LPA proton beams. Removable radiochromic films (type HD-V2) and a Thomson energy spectrometer are utilized to measure the protons. (b) Characteristics of the LPA proton bunch, exhibiting an exponentially decaying energy spectrum and energy-dependent divergence angles in the order of hundreds of mrad. (c) Determination of APL discharge timing. The timing between the current and the proton beam, influencing the focusing power of the APL on the protons, was adjusted based on simultaneous recordings of the discharge current and the electromagnetic pulses (EMPs) generated synchronously with the beam. (d) Selection of APL filling gas type. The spectral lines (the color scale represents the count from the electron-multiplying CCD used for detecting the beam signals, which is proportional to beam intensity) captured by the spectrometer after the proton beam passed through argon (left) and helium (right) plasmas indicated that argon plasma is unsuitable as a transmission medium for MeV energy LPA protons. Therefore, in our experiments, APLs based on helium plasma were exclusively used.

II. EXPERIMENTAL SETUP

The experiments were conducted at the compact laser plasma accelerator (CLAPA) of Peking University [35]. Figure 1 illustrates the experimental setup. A 0.8 J, 30 fs laser pulse was focused by a parabola to a spot with a full width at half maximum diameter of 5 μm, which contained 25% of the total energy, yielded an intensity of 3.4×10^{19} W/cm^2. The laser targeted a 7 μm thick aluminum sheet at a 30° angle relative to the target's normal direction, using a target normal sheath acceleration (TNSA) [36] mechanism to accelerate protons. Detected by radiochromic film (RCF) stacks [see Fig. 1(b)], the laser-accelerated proton pulses featured broad exponentially decreasing spectra with cutoff energies of 4 MeV and an energy-dependent half-opening angle of up to 200 mrad.

Following a vacuum drift at a millimeter scale, the proton beams were directed into either a C-APL or a RV-APL for focusing. The APL was filled with gas at pressures ranging from 1 to 100 torr through inlets connected to an external gas bottle and a flow regulator. Two perforated electrodes were positioned at both ends of the APL to supply a 15 kV voltage, which ionized the gas into plasma and generated a sinusoidal-like discharge current through the plasma, as shown by the red line in Fig. 1(c). This current provides a high-gradient focusing magnetic field for the proton beam.

The magnitude of the current experienced by the proton beam was ascertained by simultaneously recording the discharge current waveform and instant electromagnetic pulse (EMP) on one oscilloscope. The EMP originates from the hot electrons and target currents by the interaction between the laser and the solid target [37,38]. The peak moment of the EMPs represents the instant when the proton beam was generated [shown by the star in Fig. 1(c)]. In conjunction with a versatile digital delay/pulse generator (DG645), fine temporal synchronization was achieved. This device facilitated the control of the delay between the μs discharge current generation and the arrival of the ps-pulsed proton beam, thus enabling precise adjustment of the focusing field experienced by the proton beam.

Plasma with large atomic numbers, such as Ar plasma, has been demonstrated to be a medium capable of constructing a uniform current distribution, implying a linear magnetic field for proton beams [28,39]. This is attributed to the relatively low rates of thermal transfer between electrons and ions as well as the ion thermal conductivity, both of which are inversely proportional to the atomic number [40]. However, the scattering of the beam by plasma also increases with the atomic number [41–44], which must be taken into consideration for the MeV energy LPA protons used in our experiments. We experimentally tested APLs prefilled with either 10 torr of Ar or He gas. Following ionization and proton transmission when the current dropped to 0 A, the resulting energy spectral lines, as measured by the Thomson spectrometer and depicted in Fig. 1(d), were observed. After passing through Ar plasma, the proton beam density decreased to one-third of that passing through an empty channel, while passing through lighter He plasma, the beam density remained largely unchanged. This suggests that Ar plasma is less suitable as a transmission medium for MeV energy LPA protons. Consequently, our experiments exclusively utilized He plasma-based APLs.

The trajectories of the protons in C-APLs can be described by Hill's equation [45]:

$$\mathrm{d}^2 r/\mathrm{d}z^2 + Kr = 0, \tag{2}$$

where $K = qk/(m\gamma\beta c)$, q is the proton charge, $k = \partial B/\partial r = \mu_0 I/2\pi R^2$ (in an ideal case) is the magnetic field gradient, m is the proton mass, γ is the Lorentz factor, $\beta = v/c$ with v being the proton velocity, and c is the speed of light. As described in Ref. [34], the aperture radius $R(z)$ of the RV-APL along the longitudinal position z is consistent with the trajectory of the beam envelope, also conforming to Eq. (2). Therefore, it has the following form:

$$\frac{\mathrm{d}^2 R(z)}{\mathrm{d}z^2} + \frac{G}{R(z)} = 0, \qquad G = \frac{q\mu_0 I}{2\pi m\gamma\beta c}. \tag{3}$$

The specific value of $R(z)$ and its corresponding collection angle $\theta_{\text{RV-APL}} \approx R'(z=0)$ are determined by the aimed focusing energy E, current I, the designed object distance l_{drift1} (the distance between the object point and the entrance of APL) and image distance l_{drift2} (the distance between the focus and the exit of APL). For instance, with $E = 1$ MeV, $l_{\text{drift1}} = 6$ mm and $l = 3$ cm, the variation of $\theta_{\text{RV-APL}}$ with the current I and image distance l_{drift2} is depicted in Fig. 2(b). Figure 2(a) presents the collection angle results of the C-APL for comparison. Under equivalent settings of current and image distance, the collection angle of the RV-APL is approximately 1.5 times that of the C-APL. For the same target collection angle, the current required for the RV-APL is around 0.4 times that of the C-APL.

In this experiment, with $I = 200$ A and $l_{\text{drift2}} = 10$ cm, the estimated collection angle for the C-APL is 11 mrad, while the RV-APL can achieve up to 17 mrad. The radius of the C-APL remains constant at 400 μm, whereas the wall shape of the RV-APL, as shown by the black solid line in Fig. 2(d), varies in radius from 170 to 450 μm. This capillary was produced using 3D printing methods [46], employing HTL photosensitive resin, a commercial high-temperature resistant polymer semitransparent to visible light. Although we aim for a uniform distribution of discharge current in the APLs, the actual current density distribution is influenced by effects such as Joule heating and wall cooling [40,47,48], making it dependent on both the spatial coordinates (r, z) and time t. By employing the finite element solver package COMSOL Multiphysics, we constructed a time-dependent two-dimensional axisymmetric r-z discharge model [34].

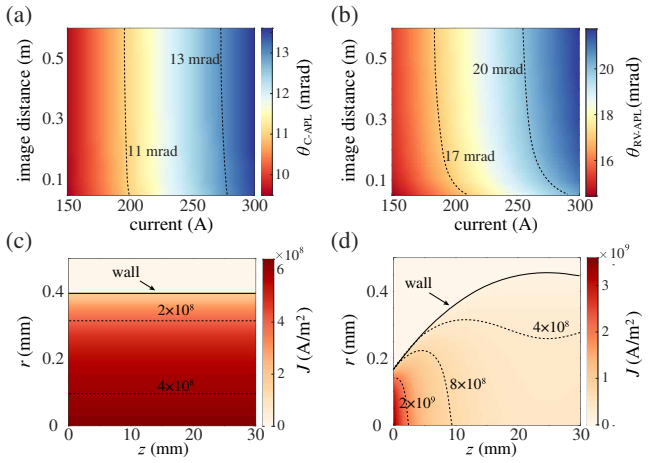

FIG. 2. C-APL's (a) and RV-APL's (b) collection angles θ with $E = 1$ MeV, $l_{\text{drift1}} = 6$ mm, and $l = 3$ cm while the capillary discharge current and the aimed image point are varied. When the current I is set at 200 A and the image distance l_{drift2} is 10 cm, the walls of C-APL and RV-APL are determined as the black solid lines shown in (c) and (d), respectively. Additionally, their corresponding simulated r-z current density distributions are provided.

We obtained simulated results for the current density distribution in both C-APL and RV-APL at the moment corresponding to a current of 200 A, as depicted in Figs. 2(c) and 2(d), respectively. Due to its smaller entrance radius, the RV-APL exhibits a higher current density near the entrance. It is calculated that the on-axis magnetic field gradient at the entrance reaches 2.2 kT/m, whereas the on-axis magnetic field gradient of C-APL is only 0.4 kT/m. This allows the RV-APL to promptly confine protons with a larger divergence angle range.

III. EXPERIMENTAL RESULTS

After passing through the APL, the proton beam traveled a distance of 2–10 cm to a series of RCF stacks, for measurements of quasimonoenergetic (1 ± 0.2 MeV) charge distribution and beam envelope evolution along its path. Figures 3(a)–3(c) sequentially display the beam spot signals at various longitudinal positions after traversing an empty capillary and under the focusing effects of the C-APL and RV-APL, respectively. In the empty capillary, the proton beam continuously diverged, with the beam density inversely proportional to the square of the drift distance. However, under the focusing influence of the APLs, beam divergences were rapidly constrained. For example, on the z plane located 5 cm from the capillary exit, the beam spot diameter decreased to one-fifth of its unfocused state, and the beam density increased by approximately an order of magnitude. Relative to the C-APL, the RV-APL further enhanced the beam density by 1.1 times. By comparing the total charge within the beam spot to the initial proton source charge, the transmission efficiency of the RV-APL for the 1 MeV proton fraction was determined to be 1.9%, which is 2.0 times that of the C-APL, significantly improving beam collection capability. Analyzing the beam spot size $\sigma_{(r,\text{FWHM})}$ across various longitudinal planes yields the motion envelope of the protons, as illustrated in Figs. 3(d)–(f). At a distance of 10 cm from the exit of the APL, the minimum $\sigma_{(r,\text{FWHM})}$

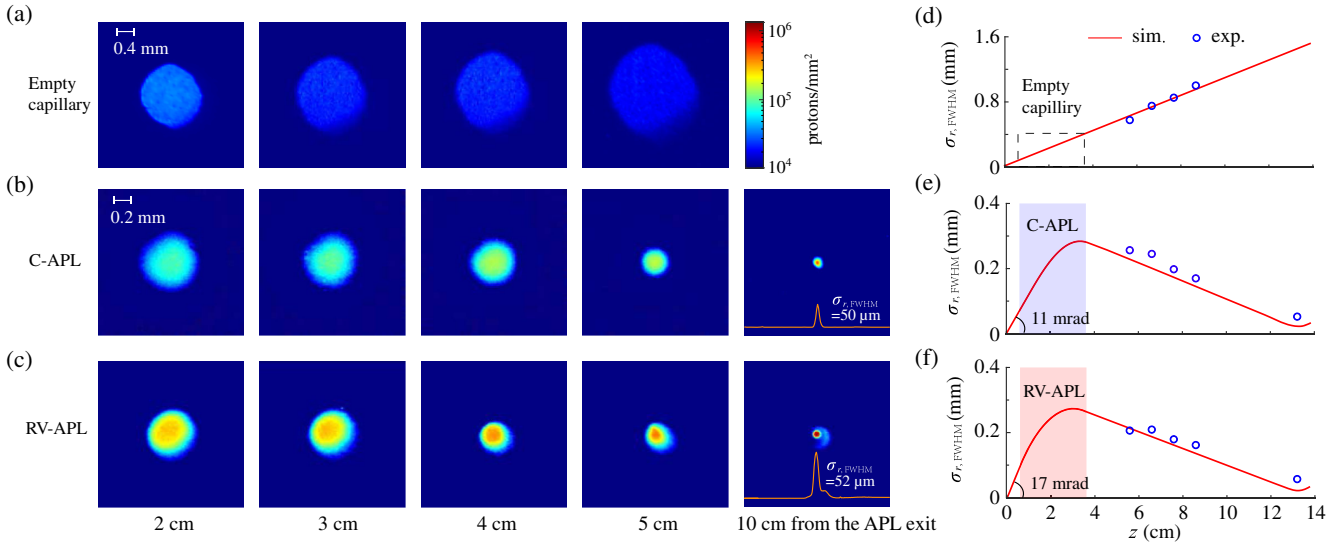

FIG. 3. (a)–(c) The transverse charge distribution and (d)–(f) beam envelope evolution of 1 MeV quasi-monoenergetic proton beam obtained by the RCFs located 2–10 cm downstream of APLs. Specifically, (a) and (d) represent the lens-off case, (b) and (e) illustrate the focusing scenario with the C-APL, while (c) and (f) demonstrate the focusing effect of the RV-APL. The red lines in (d)–(f) represent simulation results, while the blue circles denote experimental values. It is evident that the RV-APL significantly outperforms the C-APL in terms of beam collection capability.

focused by the APLs were measured to be around 50 μm. In contrast, the unfocused beam diverged excessively at this point, and the beam density failed to reach the detection threshold of the RCFs. The red curves in Figs. 3(d)–3(f) represent simulated trajectories based on the current distribution in Figs. 2(c) and 2(d), and the experimental values match the simulation values well.

By removing the RCFs, the proton beam was transported further to the Thomson spectrometer placed 15 cm away from the target with a receiving angle of ±5 mrad for energy detection. In the absence of APL, the proton source generated a spectrum with exponentially decreasing particle counts as energy increased, as shown in Fig. 4(a). When APLs were employed with a current of 200 A, due to the chromatic properties of the APLs, 2 MeV protons were focused on the spectrometer's detection plane, while protons with energies less and greater than 2 MeV were, respectively, overfocused and underfocused. This created a "bow-tie" shaped signal with stronger middle and weaker ends, as seen in Figs. 4(b) and 4(c). Comparing the beam intensities corresponding to the C-APL and RV-APL with the proton source, their gain factors η are shown in Fig. 4(d). The peak of the energy-dependent proton flux increase at 2 MeV for the RV-APL shows nearly 11 times more protons per area compared to the case without lenses and is 1.9 times that of the C-APL. This is consistent with the RCF measurements. If we define the energy achromatic range of the APL as 80% of the maximum η value, then the achromatic ability of the C-APL is 30%, while that of the RV-APL is similar at 28%. Previous studies have shown that C-APLs have reduced energy dependence compared to traditional magnetic systems such as quadrupole lens groups or solenoids [16,22], and our results suggest that RV-APLs also possess this feature, making them compatible with the broad energy spectrum of LPA proton beams.

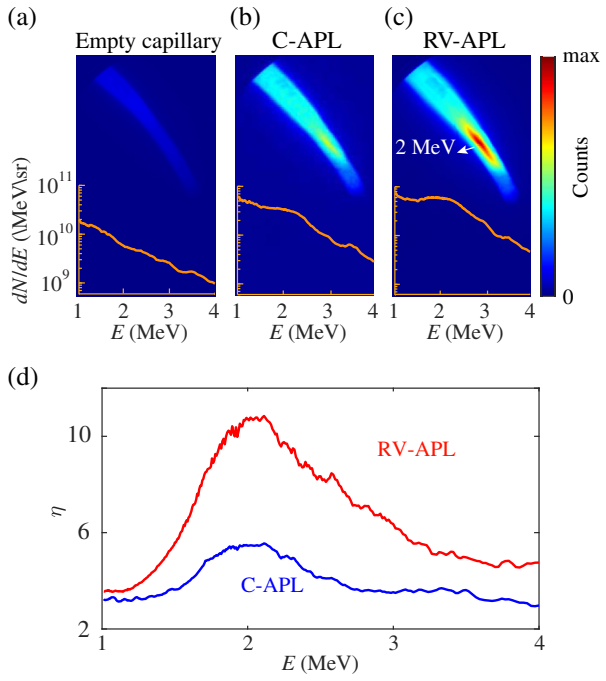

FIG. 4. The proton energy spectra detected by the Thomson spectrometer after passing through (a) an empty capillary, (b) the C-APL, or (c) the RV-APL, along with (d) the calculated beam intensity gain η corresponding to both the C-APL and RV-APL.

IV. CONCLUSIONS AND OUTLOOKS

In conclusion, we presented an experimental investigation of a radius-varying discharge capillary active plasma lens for collecting wide-angle, broad-spectrum proton beams generated by laser plasma accelerators, demonstrating an enhanced acceptance range. Direct charge measurements with RCFs revealed that RV-APL, benefiting from its optimized geometric design, effectively focuses MeV-level proton beams over centimeter distances. It exhibited a 1.5-fold increase in collection angle and a remarkable 2.0-fold enhancement in monochromatic transmission efficiency compared to the conventional cylindrical APL. Spectrometer measurements of the beam density for various energy protons post-APLs showed that the achromatic effect of the radius-varying APL is similar to that of the cylindrical APL, and its focusing effect is also relatively unaffected by changes in proton energy, making it suitable for transmitting LPA proton beams with a wide energy distribution.

Expanding the RV-APL aperture could further increase its acceptance angle, potentially comparable to traditional magnetic systems, yet with a significantly smaller volume. On the one hand, this can be achieved by appropriately increasing both the physical aperture of the capillary and the current. On the other hand, RV-APL based on Ar or other plasmas with higher atomic numbers can also be used when transmitting higher-speed proton beams that are almost unaffected by scattering. This approach would allow the current density inside the APL to approach an ideal uniform distribution [28], thereby extending the effective aperture range. A simple estimation suggests that a RV-APL with a radius varying from 0.5 to 1.5 mm and carrying a 9 kA current could achieve the collection of a 100 MeV proton beam within ±50 mrad (conversely, a C-APL would need a current of 21 kA for the same collection angle). This capability positions the RV-APL as a potential core collection component in tumor radiotherapy beamlines using LPA proton beams. The development of such compact, high-efficiency beam optical devices is a crucial step toward advancing truly miniaturized accelerators for practical applications.

ACKNOWLEDGMENTS

This work was supported by the National Natural Science Foundation of China (Grants No. 12122501, No. 11975037, No. 61631001, and No. 11921006), and the National Grand Instrument Project (No. 2019YFF01014404).

[1] A. Maksimchuk, S. Gu, K. Flippo, D. Umstadter, and V. Y. Bychenkov, Phys. Rev. Lett. **84**, 4108 (2000).

[2] I. J. Kim, K. H. Pae, I. W. Choi, C.-L. Lee, H. T. Kim, H. Singhal, J. H. Sung, S. K. Lee, H. W. Lee, P. V. Nickles *et al.*, Phys. Plasmas **23**, 070701 (2016).

[3] A. Higginson, R. Gray, M. King, R. Dance, S. Williamson, N. Butler, R. Wilson, R. Capdessus, C. Armstrong, J. Green *et al.*, Nat. Commun. **9**, 724 (2018).

[4] S. Steinke, J. Bin, J. Park, Q. Ji, K. Nakamura, A. Gonsalves, S. Bulanov, M. Thévenet, C. Toth, J.-L. Vay *et al.*, Phys. Rev. Accel. Beams **23**, 021302 (2020).

[5] S. V. Bulanov, J. J. Wilkens, T. Z. Esirkepov, G. Korn, G. Kraft, S. D. Kraft, M. Molls, and V. S. Khoroshkov, Phys. Usp. **57**, 1149 (2014).

[6] J. Bin, L. Obst-Huebl, J.-H. Mao, K. Nakamura, L. D. Geulig, H. Chang, Q. Ji, L. He, J. De Chant, Z. Kober *et al.*, Sci. Rep. **12**, 1484 (2022).

[7] Y. Gao, R. Liu, C.-W. Chang, S. Charyyev, J. Zhou, J. D. Bradley, T. Liu, and X. Yang, J. Appl. Clin. Med. Phys. **23**, e13790 (2022).

[8] G. Yang, C. Lu, Z. Mei, X. Sun, J. Han, J. Qian, Y. Liang, Z. Pan, D. Kong, S. Xu *et al.*, Front. Cell Dev. Biol. **9**, 672693 (2021).

[9] M. Fuchs, R. Weingartner, A. Popp, Z. Major, S. Becker, J. Osterhoff, I. Cortrie, B. Zeitler, R. Hörlein, G. D. Tsakiris *et al.*, Nat. Phys. **5**, 826 (2009).

[10] D. Carroll, P. McKenna, O. Lundh, F. Lindau, C.-G. Wahlström, S. Bandyopadhyay, D. Pepler, D. Neely, S. Kar, P. Simpson *et al.*, Phys. Rev. E **76**, 065401 (2007).

[11] F. Nürnberg, M. Schollmeier, E. Brambrink, A. Blažević, D. Carroll, K. Flippo, D. Gautier, M. Geißel, K. Harres, B. Hegelich *et al.*, Rev. Sci. Instrum. **80**, 033301 (2009).

[12] F. Romano, F. Schillaci, G. Cirrone, G. Cuttone, V. Scuderi, L. Allegra, A. Amato, A. Amico, G. Candiano, G. De Luca *et al.*, Nucl. Instrum. Methods Phys. Res., Sect. A **829**, 153 (2016).

[13] F. Kroll, F.-E. Brack, C. Bernert, S. Bock, E. Bodenstein, K. Brüchner, T. E. Cowan, L. Gaus, R. Gebhardt, U. Helbig *et al.*, Nat. Phys. **18**, 316 (2022).

[14] J. Zhu, M. Wu, K. Zhu, Y. Geng, Q. Liao, D. Li, T. Yang, M. Easton, C. Li, X. Xu *et al.*, Phys. Rev. Accel. Beams **23**, 121304 (2020).

[15] M. Schollmeier, S. Becker, M. Geißel, K. Flippo, A. Blažević, S. Gaillard, D. Gautier, F. Grüner, K. Harres, M. Kimmel *et al.*, Phys. Rev. Lett. **101**, 055004 (2008).

[16] J. Van Tilborg, S. Barber, C. Benedetti, C. Schroeder, F. Isono, H.-E. Tsai, C. Geddes, and W. Leemans, Phys. Plasmas **25**, 056702 (2018).

[17] W. K. H. Panofsky and W. R. Baker, Rev. Sci. Instrum. **21**, 445 (1950).

[18] F. Dothan, H. Riege, E. Boggasch, and K. Frank, J. Appl. Phys. **62**, 3585 (1987).

[19] E. Boggasch, J. Jacoby, H. Wahl, K.-G. Dietrich, D. Hoffmann, W. Laux, M. Elfers, C. Haas, V. Dubenkov, and A. Golubev, Phys. Rev. Lett. **66**, 1705 (1991).

[20] E. Boggasch, A. Tauschwitz, H. Wahl, K.-G. Dietrich, D. Hoffmann, W. Laux, M. Stetter, and R. Tkotz, Appl. Phys. Lett. **60**, 2475 (1992).

[21] E. Boggasch, B. Heimrich, and D. Hoffmann, Nucl. Instrum. Methods Phys. Res., Sect. A **336**, 438 (1993).

[22] J. Van Tilborg, S. Steinke, C. Geddes, N. Matlis, B. Shaw, A. Gonsalves, J. Huijts, K. Nakamura, J. Daniels, C. Schroeder *et al.*, Phys. Rev. Lett. **115**, 184802 (2015).

[23] M. Borghesi, A. Mackinnon, D. H. Campbell, D. Hicks, S. Kar, P. K. Patel, D. Price, L. Romagnani, A. Schiavi, and O. Willi, Phys. Rev. Lett. **92**, 055003 (2004).

[24] P. Vrba and M. Vrbová, Contrib. Plasma Phys. **40**, 581 (2000).

[25] T. Yang, H. Cheng, Y. Yan, M. Wu, D. Li, Y. Li, Y. Xia, C. Lin, and X. Yan, Phys. Rev. Accel. Beams **24**, 031301 (2021).

[26] R. Pompili, M. Anania, M. Bellaveglia, A. Biagioni, S. Bini, F. Bisesto, E. Brentegani, G. Castorina, E. Chiadroni, A. Cianchi *et al.*, Appl. Phys. Lett. **110**, 104101 (2017).

[27] R. Pompili, M. Anania, M. Bellaveglia, A. Biagioni, S. Bini, F. Bisesto, E. Brentegani, F. Cardelli, G. Castorina, E. Chiadroni *et al.*, Phys. Rev. Lett. **121**, 174801 (2018).

[28] C. A. Lindstrøm, E. Adli, G. Boyle, R. Corsini, A. Dyson, W. Farabolini, S. Hooker, M. Meisel, J. Osterhoff, J.-H. Röckemann *et al.*, Phys. Rev. Lett. **121**, 194801 (2018).

[29] E. Chiadroni, M. Anania, M. Bellaveglia, A. Biagioni, F. Bisesto, E. Brentegani, F. Cardelli, A. Cianchi, G. Costa, D. Di Giovenale *et al.*, Nucl. Instrum. Methods Phys. Res., Sect. A **909**, 16 (2018).

[30] S. Barber, J. Bin, A. Gonsalves, F. Isono, J. van Tilborg, S. Steinke, K. Nakamura, A. Zingale, N. Czapla, D. Schumacher *et al.*, Appl. Phys. Lett. **116**, 234108 (2020).

[31] A. Marocchino, M. Anania, M. Bellaveglia, A. Biagioni, S. Bini, F. Bisesto, E. Brentegani, E. Chiadroni, A. Cianchi, M. Croia *et al.*, Appl. Phys. Lett. **111**, 184101 (2017).

[32] J. Van Tilborg, S. Barber, H.-E. Tsai, K. Swanson, S. Steinke, C. Geddes, A. Gonsalves, C. Schroeder, E. Esarey, S. Bulanov *et al.*, Phys. Rev. Accel. Beams **20**, 032803 (2017).

[33] S. Steinke, J. Van Tilborg, C. Benedetti, C. Geddes, C. Schroeder, J. Daniels, K. Swanson, A. Gonsalves, K. Nakamura, N. Matlis *et al.*, Nature (London) **530**, 190 (2016).

[34] Y. Yan, T. Yang, Z. Guo, H. Cheng, Y. Li, Y. Fang, Y. Xia, Q. He, C. Li, M. Huang *et al.*, Nucl. Instrum. Methods Phys. Res., Sect. A **1057**, 168737 (2023).

[35] Y.-X. Geng, Y.-R. Shou, J.-G. Zhu, X.-H. Xu, M.-J. Wu, P.-J. Wang, D.-Y. Li, R.-H. Hu, D.-H. Wang, Y.-Y. Zhao *et al.*, Chin. Phys. Lett. **35**, 092901 (2018).

[36] K. Zeil, J. Metzkes, T. Kluge, M. Bussmann, T. E. Cowan, S. Kraft, R. Sauerbrey, and U. Schramm, Nat. Commun. **3**, 874 (2012).

[37] F. Consoli, V. T. Tikhonchuk, M. Bardon, P. Bradford, D. C. Carroll, J. Cikhardt, M. Cipriani, R. J. Clarke, T. E. Cowan, C. N. Danson *et al.*, High Power Laser Sci. Eng. **8**, e22 (2020).

[38] Y. Li, M. Wu, D. Li, T. Yang, H. Cheng, Y. Xia, Y. Yan, Y. Geng, Y. Zhao, C. Lin *et al.*, Phys. Plasmas **30**, 043106 (2023).

[39] K. N. Sjobak, E. Adli, R. Corsini, W. Farabolini, G. Boyle, C. A. Lindstrøm, M. Meisel, J. Osterhoff, J.-H. Röckemann, L. Schaper *et al.*, Phys. Rev. Accel. Beams **24**, 121306 (2021).

[40] N. Bobrova, A. Esaulov, J.-I. Sakai, P. Sasorov, D. Spence, A. Butler, S. M. Hooker, and S. Bulanov, Phys. Rev. E **65**, 016407 (2001).
[41] T. Peter and J. Meyer-ter Vehn, Phys. Rev. A **43**, 1998 (1991).
[42] H. Nersisyan, Phys. Rev. E **58**, 3686 (1998).
[43] E. Nardi, Y. Maron, and D. Hoffmann, Laser Part. Beams **25**, 489 (2007).
[44] H. A. Bethe, Phys. Rev. **89**, 1256 (1953).
[45] S.-Y. Lee, *Accelerator Physics* (World Scientific Publishing Company, Singapore, 2018).
[46] F. Filippi, M. Anania, A. Biagioni, E. Chiadroni, A. Cianchi, Y. Ferber, M. Ferrario, and A. Zigler, Rev. Sci. Instrum. **89**, 083502 (2018).
[47] A. Curcio, F. Bisesto, G. Costa, A. Biagioni, M. Anania, R. Pompili, M. Ferrario, and M. Petrarca, Phys. Rev. E **100**, 053202 (2019).
[48] G. J. Boyle, M. Thévenet, J. Chappell, J. Garland, G. Loisch, J. Osterhoff, and R. D'Arcy, Phys. Rev. E **104**, 015211 (2021).